Resolution independent characteristic scale dedicated to satellite images

Bin Luo,Jean-François Aujol,Yann Gousseau,Saïd Ladjal and Henri Maître *Member, IEEE.*

***Abstract*—We study the problem of finding the characteristic scale of a given satellite image. This feature is defined so that it does not depend on the spatial resolution of the image. This is a different problem than achieving scale invariance, as often studied in the literature. Our approach is based on the use of a linear scale-space and the total variation. The critical scale is defined as the one at which the normalized total variation reaches its maximum. It is shown experimentally, both on synthetic and real data, that the computed characteristic scale is resolution independent.**

I. Introduction

Scale is usually regarded as one of the most significant features for image characterization. A wide body of literature has been devoted to the examination of images at different scales, giving birth to the popular scale-space theory. Several mathematical tools have concurrently been used to perform such an analysis: mathematical morphology, wavelet decompositions, differential equations, pyramid decompositions, etc.

While scale has a clear definition in several domains of engineering (architecture, cartography, etc ...), it has a much fuzzier meaning in digital image processing. There, as in Physics, it reflects to some extent the level of refinement of the representation of the observed world [1]. In this rationale, a scale-space representation offers a series of images where details are progressively filtered, from the thinnest to the coarsest ones, each level providing an image where no detail smaller than a given size is left. This leads to the concept of characteristic scale. It is attached to a structure (object, group of objects or texture) and denotes this precise scale, in a scale-space representation, where this structure is the most easily perceived.

For thinner scales than the characteristic scale, fine details may interfere with the structure making it less salient; for coarser scales, the contrast of the structure is blurred by low pass filtering or the structure may even have disappeared. Lindeberg strongly defended this approach and, for an operational implementation, proposed an efficient definition by relating the characteristic scale to the scale where a suitable combination of derivatives assumes a local maximum [2].

In the specific case of remote sensing imaging, the ratio relating the true size of an object to its size in pixels is almost constant for a given image and is given by the resolution. In this paper, we assume that the resolution is known and we address the problem of deriving a characteristic scale that is related to the physical dimension of a scene contents. Contrarily to classical approaches in Computer Vision where characteristic scales are local measures associated to each object or sub-object (see e.g. [3]), yielding a complete scale spectrum, the scale measure considered in this paper is an average measure associated to an image or a sub-image. Indeed, satellite images present relatively large homogeneous regions for which it is of strong interest to know the mean characteristic size of objects, see Figure 1. Of course this is a simplification since such images will sometimes contain two or three predominant scales, each one visible in a certain range of resolutions.

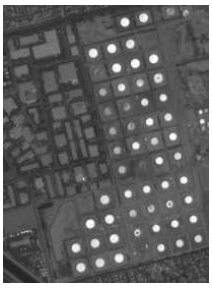

Fig. 1. An image of SPOT5 ($5m$) taken on Los Angeles, typical example of the homogeneous regions of remote sensing imaging. The oil tanks are periodically distributed in this image. We have measured manually the distance between the centers of two adjacent tanks, which is approximately $100m$.

The derivation of such a resolution independent characteristic scale was motivated by the need of the CNES (French space agency) to index very large and diverse satellite image databases. Such databases are among the fastest growing image archives and space agencies are developing indexing scheme to be able to handle them efficiently, for instance using data mining techniques, see [4]. Now, these databases are often composed of images taken at different resolutions, depending on the acquisition satellite involved. To compare the physical contents of different images, it is therefore needed to compute resolution invariant indexes. This is in particular the case for the characteristic scale, a very efficient image feature for the task of image discrimination, see [5], [6], [7]. Of course this goal is not fully achievable. In particular, characteristic scales that are small compared to the spatial resolution of the image cannot be recovered. More generally, and as can be expected, the proposed methodology will rely on some knowledge of the acquisition system, a sensible hypothesis in the case of remote sensing imaging.

Formally, the problem is as follows. There exists an underly-

B. Luo, Y. Gousseau, Saïd Ladjal and Henri Maître are with GET/Télécom Paris, CNRS UMR 5141 CNES-DLR-ENST Competence Centre, 46, rue Barrault, 75013 Paris, France.

J-F. Aujol is with CMLA, ENS Cachan, CNRS, PRES UniverSud, 61 Av. President Wilson, F-94230 Cachan, France.

ing scene f of which we know a discrete version $\tilde{f}$. Assuming we have some characteristic scale definition (to be discussed in details) $S(f)$, we wish to find an operator $\tilde{S}$ such that $\tilde{S}(\tilde{f}) = S(f)$. We shall see that this is possible when making the following assumptions. First, the resolution of $\tilde{f}$ must not be too coarse compared to the "continuous" characteristic scale $S(f)$. Second, it is assumed that $\tilde{f}$ is obtained from f through convolution with a Gaussian kernel and regular sampling. Last, the characteristic scale $S(f)$ is defined by looking at the maximum of some operator in a linear scale-space, a classical method from Computer Vision. This last assumption is of primary importance, since this specific type of scale definition enables to recover the scale even though some information has been lost in the acquisition of $\tilde{f}$.

Let us underline that the problem of deriving a characteristic scale independent of the spatial resolution is different from the classical requirement that a characteristic scale should be invariant under a change of scale. Namely, if the function $f(x, y)$ is transformed into $f(kx, ky)$, the characteristic scale $S(f)$ should be transformed into $k^{-1}S(f)$. Some works report experimental results showing that such an invariance should be enough for the purpose of computing the scale of local descriptors issued from images originating from two different sensors (see for instance Figure 1 of [8]). However, as the experiments of Section VI will show, it is our experience that without taking into consideration the impact of the sensor resolution, the derived characteristic scale is biased. Our approach therefore explicitly incorporates the sensor impulse response in the characteristic scale estimation. The scale invariant and resolution invariant approaches are compared in Section VI. In particular, we will see that our approach yields accurate results even when the convolution kernel of the imaging sensor is not Gaussian. Some preliminary results of the proposed approach were presented in [9].

The plan of the paper is the following. In Section II, we recall the classical definitions of characteristic scales. In Section III, a first definition of the characteristic scale is given, based on the definition in [2] but differing by the mathematical norm used. In Section IV, the main contribution of this paper is presented: we adapt the definition of the characteristic scale by taking into account the acquisition process in order to achieve resolution invariance. In Section V, the behavior of the proposed characteristic scale definition is studied on various synthetic images. In Section VI we test our approach on real data provided by the French space agency (CNES).

II. Classical definitions of characteristic scales

Many definitions of characteristic scales for images have been proposed in the literature. The most popular one is probably the aforementioned definition relying on linear scale-space [2], [10]. Many alternatives also relying on the use of the linear scale-space have been proposed in the field of Computer Vision, see e.g. [8]. Definitions relying on extrema of wavelet decompositions, see e.g. [11], can be put in the same category. Recently, it has been proposed to use non-linear scale-spaces in a similar way, [7]. Several alternative approaches rely on information theory: in [6] the maximum entropy between consecutive wavelet subbands, in [12] the maximum Kullback divergence after increasing filtering by diffusion equations, in [13] the maximum change of entropy, in [14] the maximum change of generalized entropy, and in [15] the maximum entropy of gray level differences are used as definitions. A third kind of approach, popular in remote sensing imaging, relies on the use of the variogram of images, see [16]. However, most methods relying on the use of second order statistics assume that images follow some specific model, such as various point processes [17] or periodic functions [18] and are not suited to complex images for which such assumptions are not realistic.

In this paper, we choose to follow the approach proposed by Lindeberg because the use of a linear scale-space naturally allows us to take the acquisition process of the image into account when computing a characteristic scale.

III. Basic tools and scale definition

In this section, we recall the models and mathematical tools to be used in this work, and give a definition of the characteristic scale of an image. Namely, we define the simplified acquisition process assumed for images, we introduce the classical linear scale-space to be used for scale characterization and we define the total variation of images. We then define the characteristic scale as the maximizer of a normalized total variation in the linear scale-space.

a) Simplified sampling scheme: We assume that the scene under study is represented by a continuous function f, and that the digital image f_r at resolution r is obtained by convolution and sampling. Moreover, it is assumed that the convolution kernel is Gaussian, with a standard deviation $\sigma = r/\alpha$ proportional to the resolution. This can conveniently be modeled as:

$$f_r = \Pi_r . (f * k_\sigma) , \tag{1}$$

where:

$$k_\sigma(x, y) = \frac{1}{2\pi\sigma^2} \exp\left(-\frac{x^2 + y^2}{2\sigma^2}\right), \tag{2}$$

and Π_r is the Dirac comb on $\mathbb{Z}^2$, that is,

$$\Pi_r = \sum_{i,j\in\mathbb{Z}} \delta_{(ir,jr)}.$$

In this context, our goal is to extract from f_r a characteristic scale related to f. Equation (1) is a rough approximation of the real acquisition process, neglecting some important aspects such as noise or contrast changes and assuming a simple form for the modulation transfer function of the imaging device. These limitations will be discussed in Sections III e) and VI c). Moreover, it will also be shown experimentally in Section VI c) that this model is accurate enough for our purpose.

b) Linear scale-space: As previously explained, the basic idea to extract characteristic scales is to track structural changes in scale spaces. In order to deal with images at various resolution (as expressed by (1)) we are naturally led to use a linear scale space [19]. For an image $f : \mathbb{R}^2 \mapsto \mathbb{R}$, its linear scale-space is a function $L : \mathbb{R}^2 \times \mathbb{R}_+ \to \mathbb{R}$ defined as:

$$L(x, y; t) = k_t * f(x, y), \tag{3}$$

where k_t is defined by Formula (2). It is easily seen that $L(.,.;\sqrt{2t})$ is a solution of the heat equation $\partial_t L = \Delta L$, with initial condition $L(.,.;0) = f$ and that, under reasonable hypotheses, it is the only solution. For this reason, $L(.,.;\sqrt{2t})$ is the classical definition of linear scale-space. However, we prefer the definition given by Formula (3) that simplifies forthcoming computations and allows to directly define a scale that is homogeneous to a distance.

Various non-linear scale-spaces could also be considered, [20], [21], [22], but we restrict ourselves to the linear one to be able to deal with resolution changes, as it will become clear soon.

c) Total variation: The structural changes to be quantified in the linear scale-space are due to the objects present in the scene. These objects disappear as the scale increases. The basic idea of the proposed approach is to quantify the evolution of geometric structures of the image in the linear scale-space. Therefore, we consider the total variation (TV) [23] of images, defined (when the image is regular enough) as $TV(f) = \int |\nabla f|$. Indeed, the semi-norm TV is related to the geometry of the image through the coarea formula. Writing $E_\lambda = \{x : f(x) \geq \lambda\}$ for the upper level sets of f, if f is regular enough, one has

$$TV(f) = \int_{\mathbb{R}} \text{per}(E_\lambda) d\lambda.$$

This implies that for a binary image, $TV(f)$ is equal to the perimeter of the objects multiplied by their contrast.

d) Scale definition: Following the general approach of [2], we define the characteristic scale of an image as the maximizer of a suitably normalized differentiable operator. To deal with the geometric contents of the image, we choose to use a normalized total variation, $NTV(f;t) = \phi(t)\, TV\,(k_t * f)$. The main idea is that the normalization term must compensate the decrease of the total variation caused by Gaussian smoothing. We denote by $t_{\max}$ the maximizer of the normalized TV over t. A natural requirement on $t_{\max}$ is that $t_{\max}(f) = s t_{\max}(f^s)$, where $f^s(\mathbf{x}) = f(s\mathbf{x})$. In Appendix C and D, we show that this implies $\phi(t) = At^B$ and that $\phi(t) = t$ is a good choice for numerical reasons. That is, we define

$$NTV(f;t) = t\, TV\,(k_t * f) = t \int |\nabla k_t * f|, \qquad (4)$$

and

$$t_{\max} = \text{argmax}_{\mathbb{R}_+^*} NTV(f;t). \qquad (5)$$

This is in fact a special case of the normalization proposed by Lindeberg [2] for differential operators. In Appendix B, we comment on the possibility of using other differential operators than the total variation.

e) Robustness to noise and contrast change: Observe that the characteristic scale definition (5) is invariant under linear contrast changes. Indeed, if $f \to af + b$, with $a > 0$, then $NTV(f;t) \to a.NTV(f;t)$. This is very convenient when dealing with satellite images, since contrast changes due to atmospheric perturbations are often approximated by an affine transform. This invariance is also sufficient when computing the scale of scenes made of objects with similar intensities on a homogeneous background. However, the method is of course not fully contrast invariant, which could be a problem in the case of objects with very different intensities.

Notice also that due to the use of the linear scale-space in the computation of $t_{\max}$, noise is not an issue. Indeed, the size of objects contributing to the characteristic scale is much larger than one pixel. Therefore, any reasonable noise is removed from the scale-space image corresponding to $t_{\max}$.

Recall now that we are interested in discrete images obtained from f through Equation (1). In the next section, we show how to adapt the definition of characteristic scale in this context.

IV. Resolution invariance

The purpose of this section is to derive a method to ensure that the computed characteristic scale does not depend upon the resolution of the image.

a) Taking the acquisition process into account: Recall that f is a continuous function corresponding to a given scene. Since we assume that the acquisition system performs a convolution by a Gaussian kernel k_σ followed by a sampling at rate $r = \alpha\sigma$, we write:

$$f_r = \Pi_r.(f * k_{r/\alpha}),$$

where f_r is the sampled version of f at resolution r. The parameter α is a characteristic of the acquisition process.

Denoting by $\tilde{k}_t$ the discrete version of the Gaussian kernel with standard deviation t (t expressed in pixels), we have $\tilde{k}_t \approx k_{rt}$ (up to some normalization constant which can be dropped). Let us define the discrete scale-space as:

$$f_{r,t} = \tilde{k}_t \tilde{*} f_r = \tilde{k}_t \tilde{*} \left(\Pi_r.\left(k_\sigma * f\right)\right) \approx \Pi_r.\left(k_{rt} * \left(k_\sigma * f\right)\right). \qquad (6)$$

where $\tilde{*}$ is the discrete convolution. The last approximation means that inverting convolution and sampling is possible, at least for non-aliased images such as $k_\sigma * f$. In Figure 2, we test the validity of this assumption on a real image. The result fully supports the hypotheses. In addition we can assume (for well-sampled images) that the total variation of the continuous and discrete versions are the same up to a normalization due to the zooming of factor r (this will be confirmed by the numerical experiments in the following sections). This leads to:

$$TV(f_{r,t}) \approx \frac{1}{r} TV(k_{rt} * k_\sigma * f) = \frac{1}{r}\, TV\left(k_{\sqrt{r^2t^2+\sigma^2}} * f\right). \qquad (7)$$

b) Normalization choice: A normalization of the discrete total variation is now needed in order to relate it to the continuous normalized total variation NTV (defined in Equation (4)). Let us define:

$$G_r(t) = h(t)\, TV\left(f_{r,t}\right), \qquad (8)$$

where the normalization factor $h(t)$ is to be chosen. Similarly to Equation (4), we may define:

$$t_{\max_r} = \text{argmax}_{\mathbb{R}_+^*} G_r(t). \qquad (9)$$

Proposition: If we choose in Equation (8):

$$h(t) = \sqrt{t^2 + \frac{1}{\alpha^2}} \qquad (10)$$

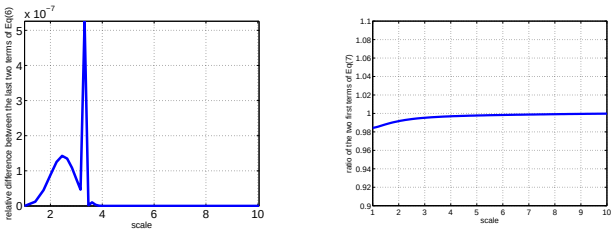

(a) (b)

Fig. 2. Validation test of Equations (6) and (7). Figure (a) shows the relative difference between the total variation of the last two terms of Equation (6) as a function of σ, where f is the image (b) of Figure 11. The relative difference does not exceed 10^{-6}. In Figure (b) is shown the ratio between the two first terms of Equality (7); this ratio varies between 0.98 and 1. This experiment validates the assumption of Equation (7).

(with $\alpha = r/\sigma$ characteristic of the acquisition process), then the following relation holds ($t_{\max}$ being defined by (5)):

$$t_{\max} \approx \sqrt{r^2 t_{\max_r}^2 + \sigma^2} \approx r\sqrt{t_{\max_r}^2 + \frac{1}{\alpha^2}}. \qquad (11)$$

Proof:

Using Equation (7):

$$\begin{aligned} G_r(t) &\approx \frac{1}{r} h(t)\, TV\left(k_{\sqrt{r^2t^2+\sigma^2}} * f\right) \\ &= \frac{1}{r}\frac{h(t)}{\sqrt{r^2t^2+\sigma^2}}\, NTV\left(f; \sqrt{r^2t^2+\sigma^2}\right). \end{aligned}$$

Hence:

$$G_r(t) \approx \frac{1}{r^2}\frac{h(t)}{\sqrt{t^2+\frac{1}{\alpha^2}}}\, NTV\left(f; \sqrt{r^2t^2+\sigma^2}\right). \qquad (12)$$

Since $h(t)$ is given by (10), we then obtain:

$$G_r(t) \approx \frac{1}{r^2}\, NTV\left(f; \sqrt{r^2t^2+\sigma^2}\right) \qquad (13)$$

We thus deduce (11) from (5) and (9). ■

c) Practical considerations: For a discrete image at resolution r we measure $t_{\max_r}$ and derive the value of $t_{\max}$ using Equation (11). Notice that it is impossible to find a characteristic scale $t_{\max}$ smaller than σ (which is comparable to r). More generally, when the resolution of the image is larger than the actual characteristic scale $t_{\max}$ the computation becomes unreliable. Experiments show that $t_{\max}$ is retrievable as long as $r < t_{\max}$.

Of course, a general image can contain several characteristic scales. A scale can therefore be a characteristic of some scene for a specific range of resolution. As will be seen in the numerical experiments section, the characteristic scale $t_{\max}$ that we compute with Equation (11) corresponds to the smallest retrievable scale in the image. For instance, as shown on Figure 14(d)), the characteristic scale of the image of Roujan (see Figure 11(d)) is 0.4m (due to the details inside the fields) if the resolution r of the image is smaller than 0.4m, whereas when the resolution gets larger the characteristic scale jumps to 30m (due to the size of the fields itselves).

From now on, the values of $t_{\max}$ will be deduced from Equation (11).

d) Difference with the "naïve" normalization choice: In view of Equation (4), the intuitive normalization would not take into account the filtering process due to the change of resolution and, therefore, involve a factor t instead of $h(t)$:

$$A_r(t) = t \times TV\left(f_{r,t}\right) \qquad (14)$$

If, according to this intuition, we set $t_{\max_r}$ as $\text{argmax}_{\mathbb{R}_+^*}(A_r(t))$ and deduce $t_{\max} = r \times t_{\max_r}$, then we can check numerically that the obtained value of $t_{\max}$ will depend much more on the resolution than with the definition from Equation (11). This fact will be detailed in Section VI, see Figure 18.

Notice also that when $t \gg 1$, then the definitions from Equations (8) and (14) are equivalent. The choice of the correct normalization given by Equation (10) is important when r approaches $t_{\max}$ (that is $t_{\max_r}$ approaches 1).

V. Relating $t_{\max}$ to the geometry of the image

In this section, we investigate the link between the characteristic scale $t_{\max}$, as defined in Section III for a continuous image, and the geometric contents of the image. For this purpose, following the example in [2], we first consider various simple one-dimensional functions, for which we perform computations and numerical approximations. Then, we tackle the two-dimensional case by performing numerical simulations on discrete synthetic images. We experimentally show that, for a periodic scene with spatial period D, the critical scale defined in Equation (5) is such that $t_{\max} \approx 0.15D$. The purpose of this section is to show that the constant linking $t_{\max}$ to the period is quite stable over a variety of periodic signals, for which the notion of characteristic scale is clear. Of course, real signals are much more complicated and Section VI will deal with real satellite images.

A. Continuous one-dimensional examples

In order to consider cases with tractable computations, we define $t_{\max}$ for a one-dimensional function f as in Formula (5). For 1D signals the gradient is replaced by the derivative and k_t by a one-dimensional Gaussian in the computation of $NTV(f;t)$.

a) Sinus function: Assuming that f is a sinus of period D, restricted to $[-T,T] \subset \mathbb{R}$, it may be shown that if $T/D \to \infty$ (so that boundary effects can be neglected) then $t_{\max} \to D/2\pi \sim 0.15D$, as already mentioned in [24], [2].

b) Sum of Gaussians: Assume that f is a function defined on $[-T,T] \subset \mathbb{R}$ as:

$$f(x) = \sum_{k=-K}^{K-1} \frac{1}{\sqrt{2\pi v^2}} e^{\frac{-(x-(2k+1)D/2)^2}{2v^2}}, \qquad (15)$$

ie., f is the restriction to $[-T,T]$ of a sum of Gaussians, the spatial period of this sum being D. Assuming that $K \gg 1$ (or $T \gg D$) in order to neglect boundary effects, we obtain:

$$NTV(f;t) \approx \frac{2t}{Dq\sqrt{2\pi}}\left(1 + e^{-\frac{K^2D^2}{4q^2}} + 2\sum_{k=1}^{2K-1}(-1)^k e^{-\frac{k^2D^2}{4q^2}}\right), \qquad (16)$$

where $q = \sqrt{v^2 + t^2}$. This result is obtained by noticing that the total variation may be computed on each monotonous part. The graph of $NTV(f;t)$ as a function of t is shown on Figure 3. On Figure 4 (a), the graph of $t_{\max}$ is displayed as a function of D, v being constant. One observes that $t_{\max} \approx 0.15D$, a result very similar to the one for the sinusoidal case. Figure 4 (b) shows $t_{\max}/D$ as a function of v, D being constant. One can check that $t_{\max}/D \approx 0.15$. In this case, $t_{\max}$ is related to the period of the signal but not to the width of each Gaussian.

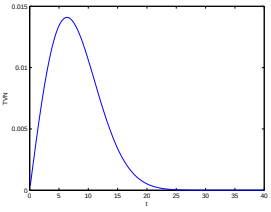

Fig. 3. Plot of $NTV(f;t)$ as a function of t, when f is a sum of Gaussians as in Equation (15), $t \in [0.1, 40]$ and $K = 10$, $D = 40$, $v = 10$. $NTV(f;t)$ reaches its maximum for $t_{\max} = 6.4$

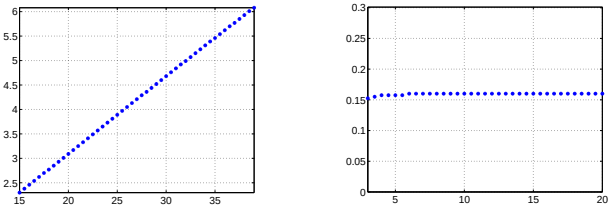

(a) $t_{\max}$ as function of D (b) $t_{\max}/D$ as a function of v

Fig. 4. Plot of $t_{\max}$ for a sum of Gaussian functions (see Equation (15)); (a):$t_{\max}$ as a function of D, with $v = 5$ (we check numerically that $t_{\max} \approx 0.15D$, D being the spatial period); (b):$t_{\max}$ as a function of v, with $D = 40$.

c) Sum of Heaviside functions: In order to investigate the sensitivity of $t_{\max}$ to the shape of "objects", we consider the following example, still in 1D to yield tractable computations: f is defined on $[-T, T]$ by

$$f(x) = \sum_{i=-K}^{K} H(x - iD) \tag{17}$$

where

$$H(x) = \begin{cases} 1, & x \in [0, v] \\ 0, & \text{otherwise} \end{cases} \tag{18}$$

with $v \in (0, D)$. Assuming that $t << D$ and $v \approx D/2$, then it may be shown using standard computations that:

$$NTV(f;t) \approx Ct \left(2\text{erf}\left(\frac{D-v}{2\sqrt{2}t}\right) - \text{erf}\left(\frac{D-v}{\sqrt{2}t}\right)\right) + \left(2\text{erf}\left(\frac{v}{2\sqrt{2}t}\right) - \text{erf}\left(\frac{v}{\sqrt{2}t}\right)\right) \tag{19}$$

where $\text{erf}(x) = \frac{2}{\sqrt{\pi}} \int_0^x e^{-u^2}$ and C is a constant.

Figure 5 (a) shows numerical computations of $t_{\max}$, taken as the zero of the derivative of Formula (19) as a function of D and Figure 5 (b) shows the plot of $t_{\max}/D$ as a function of v. Here again we obtain $t_{\max} \approx 0.15D$ and observe that $t_{\max}/D$ depends very little on v.

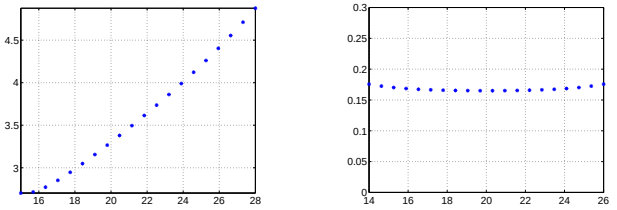

(a) $t_{\max}$ as function of D (b) $t_{\max}/D$ as a function of v

Fig. 5. $t_{\max}$ for a sum of Heaviside functions (see Equation (17)). We check numerically that $t_{\max} \approx 0.15D$ where D is the spatial period. In Figure (a) $v = 10$ and in Figure (b) $D = 40$.

To summarize, in cases a), b) and c), it may be computed or observed that $t_{\max} \approx 0.15D$, which indicates that neither the shape nor the size of the pattern seem to influence much $t_{\max}$ in the cases of 1-D functions.

B. Discrete synthetic images

In order to experimentally confirm the linear relation between $t_{\max}$ and the spatial period of signals (D in the preceding examples) in the case of images, we consider synthetic discrete periodic images using various patterns. Two instances of such images are displayed in Figure 6 (sum of Gaussians with standard deviation v) and 7 (sum of squares with width v), together with the associated graphs of NTV as functions of t. Figure 8 (a) shows the graph of $t_{\max}$ as a function of D and Figure 8 (b) shows the graph of $t_{\max}/D$ as a function of v for sums of Gaussians. Figures 9 (a) and (b) show the same quantity for sums of squares. Comparing these two figures respectively with Figure 4 and Figure 5, we conclude that the shape of patterns as well as their size have little influence on the measure. Moreover, we see that $t_{\max} \approx 0.15D$ still holds in dimension 2.

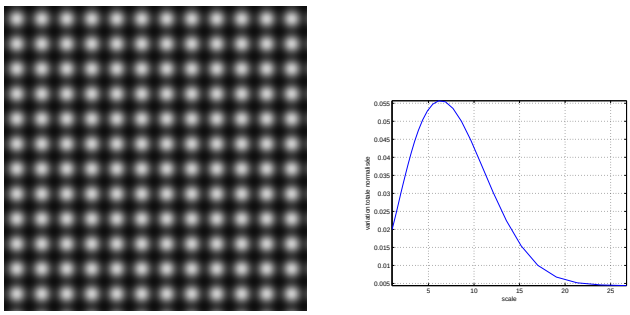

(a) Periodic sum of Gaussians (b) Graph of NTV

Fig. 6. A periodic Gaussian function with $D = 40$ and $v = 10$ (standard deviation of each Gaussian) and the graph of the corresponding normalized total variation. The maximum is reached for $t = 6.1$.

Satellite images are of course not exactly periodic. In order to check that the above empirical observation still holds in the case of randomly pertubated images, we performed the

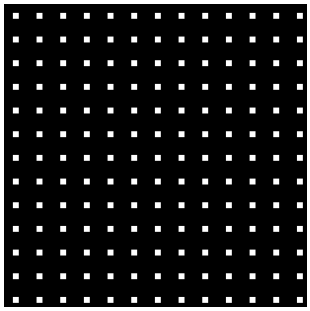

(a) Periodic sum of squares

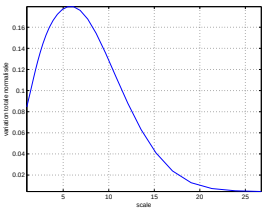

(b) Graph of NTV

Fig. 7. An image composed of squares with spatial period $D = 40$, and the side of each square equal to 10 pixels, and the graph of the corresponding normalized total variation. The maximum is reached for $t = 6.1$.

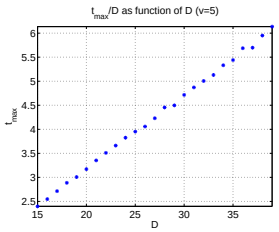

(a) $t_{\max}$ as a function of D

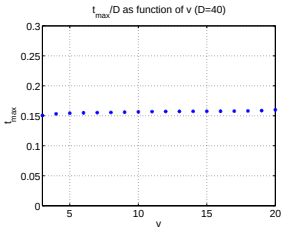

(b) $t_{\max}/D$ as a function of v

Fig. 8. (a) Graph of $t_{\max}$ as a function of D (with $v = 5$) for sums of Gaussians, we obtain $t_{\max} \approx 0.15D$; (b) Graph of $t_{\max}/D$ as a function of v (with $D = 40$) for sums of Gaussians, we obtain $t_{\max}/D \approx 0.15$.

following experiment. We start with periodic images of squares with a periodicity of $D = 20$. We perturbate the position of each square with random horizontal and vertical translations, the shifts being uniformly distributed between - 5 and 5 pixels. Moreover, the gray level of each square is random and uniformly distributed between 64 and 255. An example of such a synthetic image is shown in Figure 10(a). On Figure 10(b), values of $\frac{t_{\max}}{D}$ are displayed for 20 different realizations. The mean value of $\frac{t_{\max}}{D}$ is 0.16, which confirms the relation obtained in the periodic case.

VI. Application to satellite images

In this section several experiments are presented to demonstrate the invariance of $t_{\max}$ with respect to resolution on real images in the domain of remote sensing.

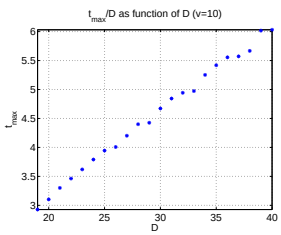

(a) $t_{\max}$ as a function of D

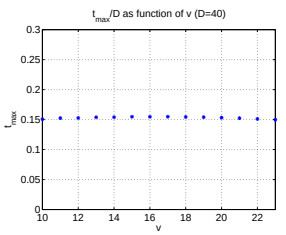

(b) $t_{\max}$ as a function of D

Fig. 9. (a) Graph of $t_{\max}$ as a function of D (with $v = 10$) for sums of squares, showing that $t_{\max} \approx 0.15D$; (b) Graph of $t_{\max}/D$ as a function of v (with $D = 40$) for sums of squares, showing that $t_{\max}/D \approx 0.15$.

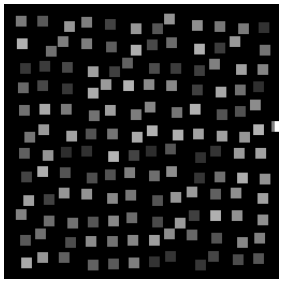

(a)

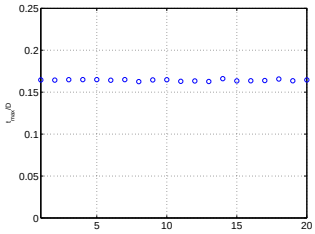

(b)

Fig. 10. (a) An example of a quasi-periodic synthetic image in which the position of each square is randomly perturbated. (b) $\frac{t_{\max}}{D}$ for 20 realizations.

At first, starting from several images with resolution equal to 25 cm, we create a series of lower resolution images using Formula (1), i.e. using a down-sampling scheme in which filtering is made using a Gaussian impulse response. We call it the ideal down-sampling.

Then, we make use of series of images provided by the CNES which precisely simulate the images which would be obtained with different sensors operating with various resolutions from a satellite, i.e. by taking into account the different effects of sampling, integration, acquisition time, etc. and therefore providing the actual impulse response of sensors.

Notice that in all the experiments presented in this section, we have used $\alpha = 1$ in Formula (11). This implicitly implies the assumption that the acquisition process is modeled by Equation (1) with $\alpha = 1$, although the real acquisition process is unknown to us.

(a) Marseille

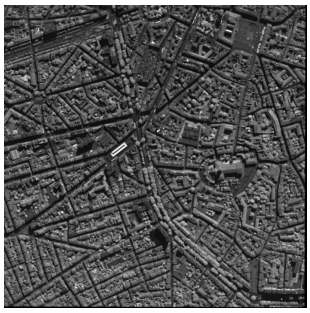

(b) Toulouse

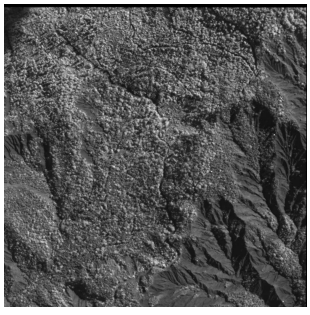

(c) Didrai

(d) Roujan

Fig. 11. Aerial images with 25 cm resolution ©CNES: (a) and (b) 2 cities with different urban tissues, (c) a forest, (d) agricultural fields.

a) Computation of $t_{\max}$ using Formula (11): On Figure 12, we display the graphs of the normalized total variation for the 4 images shown in Figure 11 (at resolution $r = 25cm$). There is at least one local maximum in each case. In the case of cities (Marseille or Toulouse), the characteristic scale is related to the size of the buildings and streets. In the case of the Didrai image (forest), the scale is related to the vegetation. Note that in the case of the Roujan image (fields), there are two local maxima, the narrow one (zoomed in Figure 12 (e)) is related to the vineyards, and the large one to the fields. Figure 13 displays a zoomed area of Figure 11 composed of vineyards. The spatial period of the vineyards D may be computed from the characteristic scale $t_{\max}$, using the relation $t_{\max} \approx 0.15D$. We find that the distance between two vineyard rows is roughly 2.7m, a result which we were able to check on the image for such a regular and periodic structure.

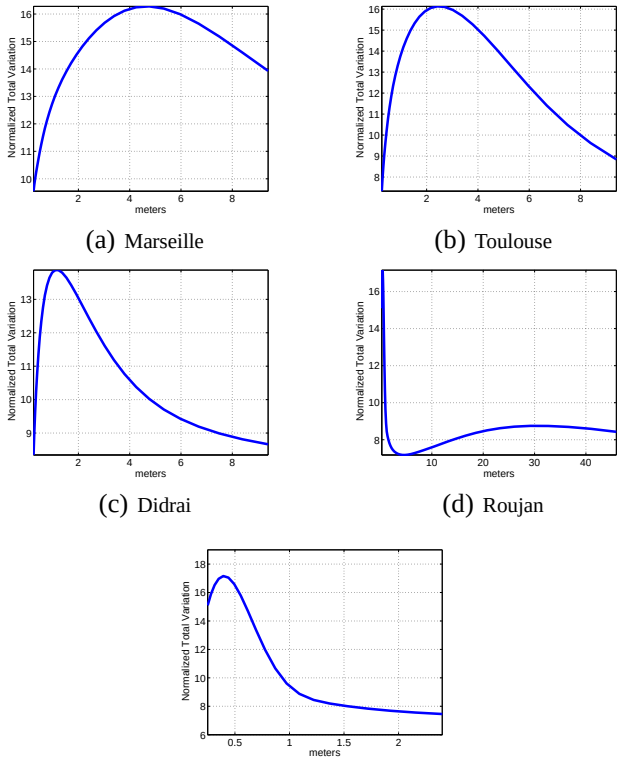

(a) Marseille (b) Toulouse (c) Didrai (d) Roujan (e) Roujan(zoomed)

Fig. 12. NTV as a function of $\sqrt{r^2t^2 + \sigma^2}$ computed for the 4 images of Figure 11 with resolution $r = 0.25m$. (a) Marseille: $t_{\max} = 4.8m$; (b) Toulouse: $t_{\max} = 2.4m$; (c) Didrai: $t_{\max} = 1.2m$; (d) Roujan: there are two local maxima. The first one at position $0.4m$, the second one at position $30m$; (e) Zoom around the first local maximum at $0.4m$ shown in (d).

b) Resolution invariance: In order to confirm that the characteristic scale extracted from the images is independent from the resolution of the sensor ($t_{\max}$ does not depend on r), we made the following experiments. For a given scene, an image g_r at resolution r is generated (using Formula (1) with $\alpha = 1$), and the maximizer $t_{\max}$ is computed. Figure 14 shows the graph of $t_{\max}$ as a function of r. As expected, it shows that $t_{\max}$ is almost constant (as long as $r < t_{\max}$).

Remark that in the case of Roujan, where two different characteristic scales are present, the plot of $t_{\max}$ is coherent with the result shown in Figure 12 (d). When the resolution r is fine enough, $t_{\max}$ is the characteristic scale corresponding to the vineyards. But when r gets larger, then the vineyards disappear (one no longer sees them in the images), and $t_{\max}$ is then related to the size of the fields.

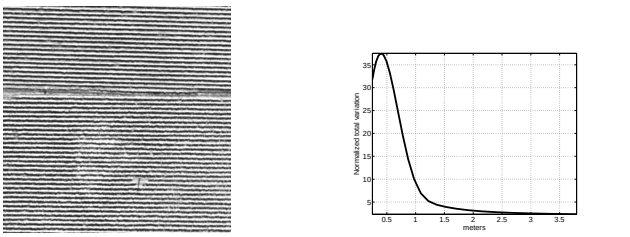

(a) Image of vineyards (b) NTV calculated on the vineyards

Fig. 13. Zoom on vineyards issued from the Roujan image displayed on Figure 11 (d). The characteristic scale appears at resolution 0.4m. Using the relation $t_{\max} \approx 0.15D$, we see that the distance D between 2 rows of vineyards is roughly 2.7m.

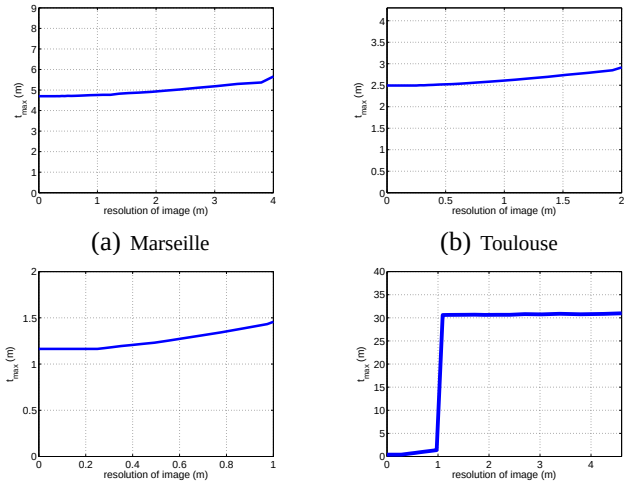

(a) Marseille (b) Toulouse (c) Didrai (d) Roujan

Fig. 14. Characteristic scales $t_{\max}$ as a function of the resolution, for the 4 scenes shown in Figure 11. The images at different resolutions are obtained by down-sampling the 25 cm images using the ideal acquisition model presented in Section IV (with $\alpha = 1$), i.e. with a Gaussian convolution kernel. Notice that the characteristic scale is almost independent from the resolution.

c) Validation of the simplified acquisition model: In order to examine the case where different sensors with different resolutions and different impulse responses are used, we take advantage of a series of images provided by the CNES, including the four images of Figure 11. For each scene, 33 images are available at resolutions ranging from 25 cm to 10.08 m (see Table I), each one taken with the exact impulse response of a real sensor. These images have been obtained by numerical simulations performed by the CNES, using aerial images and a realistic model of data acquisition. The impulse response is resolution dependent, roughly isotropic, and non-Gaussian. The use of a non-Gaussian impulse response in place of a Gaussian one makes the derivation of a relation similar to (11) difficult. However, we will see below that approximating the impulse response with a Gaussian kernel,

TABLE I
Available resolutions (meters)

0.250	0.281	0.315	0.354	0.397	0.445	0.500
0.561	0.630	0.707	0.794	0.891	1.00	1.12
1.26	1.41	1.59	1.78	2.00	2.25	2.52
2.83	3.17	3.56	4.00	4.49	5.04	5.66
6.35	7.13	8.00	8.98	10.08		

that is using Equation (11), leads to good numerical results. Due to the non-linearity of the total variation, we have no theoretical explanation for this fact.

Figure 15 shows the graph of $t_{\max}$ as a function of the resolution. Results are very similar to those of Figure 14. We observe that $t_{\max}$ is almost constant (as long as the resolution $r < t_{\max}$). Figure 16 shows four other scenes taken from the series of images provided by the CNES. The corresponding graphs of $t_{\max}$ as a function of the resolution are displayed on Figure 17; again, $t_{\max}$ is almost constant.

We conclude that even though the kernel is not Gaussian, the approximations made in section IV are still valid.

If instead of using the original relation (11) introduced in this paper, we make use of the intuitive normalization of Equation (14), we obtain the plots of Figure 18. As expected, in this case, the estimated $t_{\max}$ is much more sensitive to the resolution.

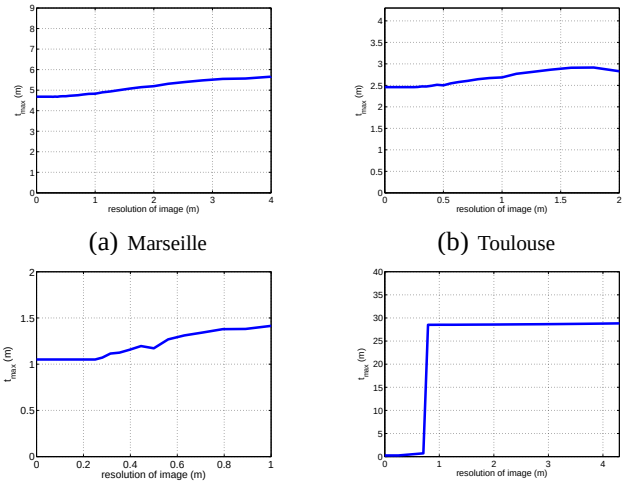

(a) Marseille (b) Toulouse (c) Didrai (d) Roujan

Fig. 15. Characteristic scale $t_{\max}$ as a function of the resolution, on the 4 scenes shown in Figure 11. The images at different resolutions are issued from the series of images provided by CNES. Even though the convolution kernel is no longer Gaussian, the characteristic scales are almost invariant when the resolution changes.

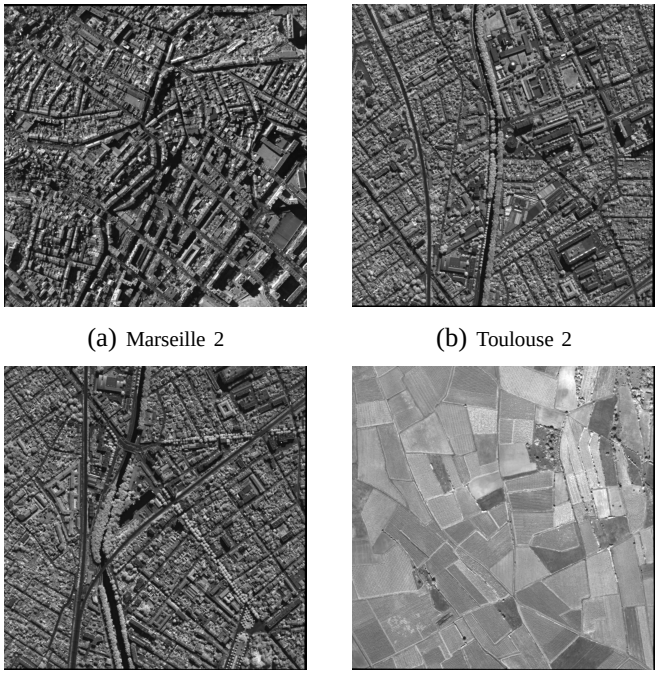

(a) Marseille 2 (b) Toulouse 2 (c) Toulouse 3 (d) Roujan 2

Fig. 16. Aerial images with 25 cm resolution ©CNES: (a), (b) (c) 3 cities with different urban tissues, (d) agricultural fields.

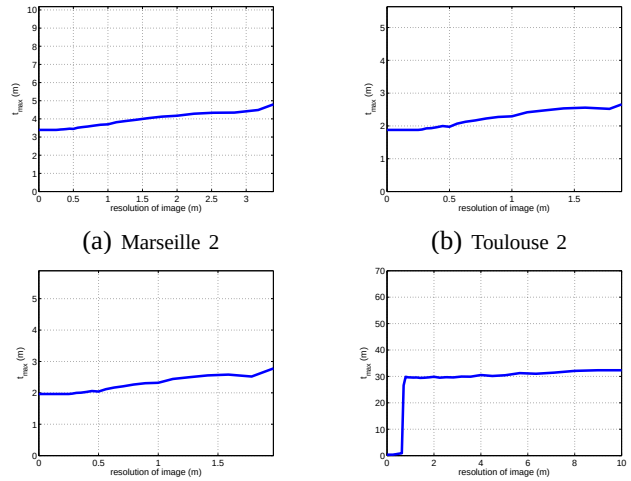

(a) Marseille 2 (b) Toulouse 2 (c) Toulouse 3 (d) Roujan 2

Fig. 17. Same experiment as in Figure 15 for the 4 scenes of Figure 16. Again the characteristic scales are almost invariant when the resolution changes.

d) Results on images taken with different captors: In Figure 1 is displayed an image of periodically distributed oil tanks. Figure 19(b) shows the graph of NTV as a function of the resolution r. The value of $t_{\max}$ is then deduced to be approximately $16m$. Recall that in Section V, we have found experimentally that $t_{\max} \sim 0.15D$, where D is the spatial period. In this case we deduce that $D \sim \frac{t_{\max}}{0.15} \sim 107m$.

To further check the captor invariance of $t_{\max}$, an image of the same region has been found in ©GoogleEarth (see Figure 20(a)). The size of a pixel of this image is roughly $8m$ (using the map scale shown on Figure 20(b)). Using formula 11, and the same value $\alpha = 1$ as before, the value of $t_{\max}$ is deduced to be approximately $14,5m$. Hence $D \approx 98$m. This is consistent with the computation made with the CNES image.

VII. Conclusion and future prospects

A new method to compute a characteristic scale for a given image has been proposed, which does not depend on the resolution (as long as the objects are larger than one pixel). This method explicitly takes into account the role of the

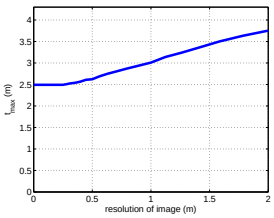

Fig. 18. Characteristic scale $t_{\max}$ as a function of the resolution, for the Toulouse image, Figure 11(b). The scale $t_{\max}$ is computed with the naive normalization given by Equation (14). Notice that the result is less invariant to resolution changes than in the case of Figure 15(b). In the range $[0.25, 2m]$, the variation of the value is 18% with the proposed method (Figure 15 (b)) and 40% with the naive normalization.

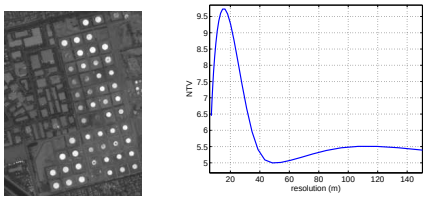

(a) (b)

Fig. 19. (a) Image on Los Angeles with oil tanks taken by SPOT5 ($5m$). ©CNES; (b) Graph of NTV as a function of the resolution. The characteristic scale $t_{\max}$ is equal to 16m.

acquisition sensor. It has been shown to be robust and stable on different images issued from the remote sensing domain. We have also shown on various examples that the position of the maximizer of the normalized TV does not depend on the object shapes, but merely on the distances between structures.

This approach is foreseen to find applications for the problem of satellite image indexing. As explained in the introduction of the paper, it is indeed a major asset that features do not depend on the resolution. In fact, the proposed resolution independent approach can be extended to other linear features such as wavelet coefficients [25]. This is the subject of ongoing work. Moreover, we expect to find the texture/geometry behavior of a scene, following ideas introduced in [26]. This could be useful for feature selection. More precisely, it could be decided in advance whether texture specific features should be used or if object recognition tools should be preferred. From a more theoretical point of view, the effect of sampling on total variation could be understood more deeply, especially when the resolution is close to $t_{\max}$.

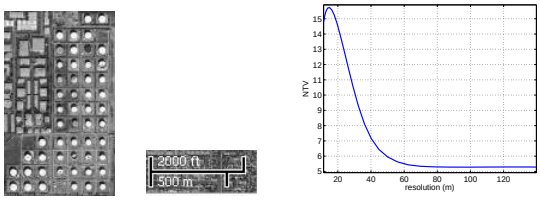

(a) (b) (c)

Fig. 20. (a) Image on Los Angeles with oil tanks. ©GoogleEarth; (b) Legend of the image, the resolution is approximately $8.06m$; (c) NTV values calculated as the function of resolution. The characteristic scale $t_{\max}$14.5m.

APPENDIX

A. Localization issue

The scale measurement we have introduced can be localized using a sliding window. The scale of a single pixel is then computed as the scale on the window centered around this pixel. To illustrate this approach, we have processed the Marseille image (see Figure 21 a). We use the image at resolution $0.707m$, with size 1440×1440. The analysis is made using a window with size 256×256, and the window is moved by 32 pixels at each step. On Figure 21 (b), we show the computed values of $t_{\max}$.

Notice in particular that $t_{\max}$ is larger in the top left corner. Looking at Figure 21 (a), one sees that this corresponds to larger buildings and structures in the original image.

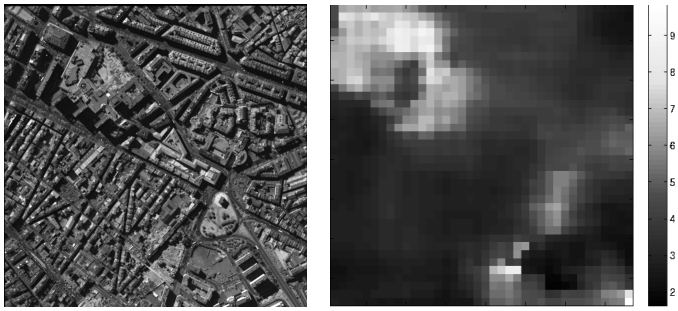

(a) (b)

Fig. 21. (a) Image of Marseille (resolution $0.707m$, size 1440×1440); (b) Image of the corresponding values of $t_{\max}$ (the larger $t_{\max}$, the whiter the gray level value in (b)).

B. Alternative definitions of $t_{\max}$

In this section, we discuss the possibility for measuring the characteristic scale with other semi-norm than the total variation. As discussed by Lindeberg [2], any normalized Gaussian derivative can be considered to achieve scale invariance. For instance, instead of using Equation (11), we could define the characteristic scale as:

$$t^l_{\max} = \arg\max_t NL(f;t) \tag{20}$$

where $NL(f;t) = t^2 \int |\nabla^2(f * k_t)|dx$. We have computed $t^l_{\max}$ both on synthetic images and remote sensing images. The results are shown in Figure 22.

On Figure 22(a), we show the values of t^l_{max}/D for various periodic images of squares with period D, as in Section V-B. It can be seen that $t^l_{\max} \sim 0.20D$. Recall that we have experimentally shown that $t_{\max}$ defined with the normalized total variation satisfies $t_{\max} \sim 0.15D$. We thus have $t^l_{\max} \sim 1.33t_{\max}$. This same relation can be observed on Figure 22(b). Nevertheless, we have decided to use the normalized total variation with Equation (11) for the two following reasons:

1) This definition is directly related to the geometric contents of a scene. Indeed, the coarea formula [23], as

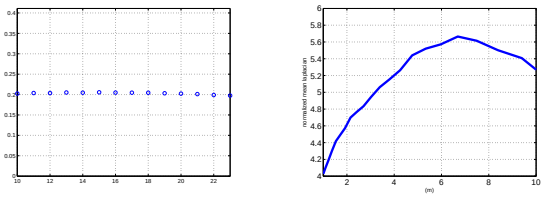

(a) (b)

Fig. 22. (a) graph of $t^l_{\max}/D$ for synthetic images (made of periodic squares with spatial period D) as a function of D where $D = 40$ (see Section V-B); (b) graph of NL computed on the image of Marseille (see Figure 11) at resolution $r = 0.25m$.

recalled in Section III, relates the total variation of an image to the perimeter of objects. A sharp object in a scene is blurred in the Gaussian scale-space. Nevertheless, the total variation of the blurred object can be seen as an approximation of its perimeter thanks to the coarea formula.

2) Using the total variation, only first order derivatives of the image are involved: there is no need to increase the complexity of the algorithm by computing higher order derivatives.

C. Normalization issue revisited

The characteristic scale of a continuous image f has been defined as:

$$t_{\max} = \text{argmax}_{\mathbb{R}_+^*} \phi(t) \int |\nabla(k_t * f)|,$$

with $\phi(t) = t$. In this section, we show why it is reasonable to choose $\phi(t) = t^B$ while the next section explains why $B = 1$ has been chosen.

Since we want $t_{\max}$ to be related to the size of objects in the image f, we naturally assume (scale-invariance) that:

$$t_{\max}(f) = s t_{\max}(f^s), \tag{21}$$

where $f^s(\mathbf{x}) = f(s\mathbf{x})$. For any $t_0 > 0$ and $s > 0$, let us define

$$F_s(t_0) = \partial_t \log \left(\phi(t) \int |\nabla f^s * k_t| \right)(t_0).$$

Equation (21) implies that

$$F_1(t_0) = 0 \Rightarrow F_s\left(\frac{t_0}{s}\right) = 0. \tag{22}$$

Now,

$$\begin{aligned} F_s\left(\frac{t_0}{s}\right) &= s\partial_t \log \left(\phi(t/s) \int |\nabla f_s * k_{t/s}| \right)(t_0) \\ &= s\partial_t \log \left(\phi(t/s) s^{-1} \int |\nabla f * k_t| \right)(t_0) \\ &= \frac{\phi'}{\phi}(t_0/s) + s\partial_t \log \int |\nabla f * k_t|(t_0) \\ &= \frac{\phi'}{\phi}(t_0/s) + s\left(F_1(t_0) - \frac{\phi'}{\phi}(t_0) \right). \end{aligned}$$

Then Equation (22) implies that

$$\frac{\phi'}{\phi}(t_0/s) = s\frac{\phi'}{\phi}(t_0),$$

and therefore $\phi(t) = At^B$ for two constants A and B to be chosen.

D. Power of normalization factor: why we set $B = 1$

The constant A does not affect $t_{\max}$. The reason why we chose $B = 1$ is essentially of a numerical nature. If B is too small, then NTV decreases very fast, implying a very small value of $t_{\max}$. This becomes a severe drawback when computing the scale of low resolution images. On the other hand, B cannot be too large. Indeed, we have checked experimentally on the images provided by the CNES that in this case the graph of NTV becomes flat and the relative error for the numerical value of $t_{\max}$ gets larger. In such a case, the localization of the extremum is not reliable. We found experimentally that setting $B = 1$ is a good compromise between these two drawbacks. Moreover, this choice is coherent with the one in [2]. As an example, Figure 23 displays the graph of NTV with $B = 1.3$ in the case of Didrai image. We may see that this value already makes it difficult to compute $t_{\max}$, whereas it is easier from Figure 12 (c).

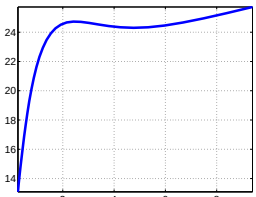

Fig. 23. NTV calculated on the image of Didrai with normalization factor $\phi(t) = t^{1.3}$.

E. Numerical issues

Numerically, the total variation $TV(I)$ of an image I is classically computed with the following expression:

$$TV(I) = \frac{1}{2} \sum_{i,j} \sqrt{(I_{i-1,j} - I_{i+1,j})^2 + (I_{i,j-1} - I_{i,j+1})^2}$$

When computing the linear scale-space, we use a logarithmic scale step, i.e.
$t \in \{1.12^n, \quad n = 0, 1, \dots\}$, in order to preserve the precision at small scales and to speed up the computation at large scales.

In order to increase the speed of the Gaussian convolution, the semi group property of the Gaussian kernel is used. The complexity of the algorithm for computing $t_{\max}$ is $O(N)$ (N is the number of pixels). On a PIV 3.2GHz machine with 1024M memory, the computation time of $t_{\max}$ for an image with size of 1024×1024 pixels is about $25s$ (where maximal scale is 37).

ACKNOWLEDGMENT

We thank the CNES for providing us with the images, and Alain Giros (CNES) and Mihaï Datcu (DLR) for fruitful discussions.

REFERENCES

[1] R. B. Fisher, K. Dawson-Howe, A. Fitzgibbon, C. Robertson, and E. Trucco, *Dictionnary of Computer Vision and Image Processing*. Wiley, 2005.

[2] T. Lindeberg, "Feature detection with automatic scale selection," *Int. J. of Computer Vision*, vol. 30, pp. 79–116, 1998.

[3] D. Lowe, "Distinctive image features from scale-invariant keypoints," *International Journal of Computer Vision*, vol. 60, no. 2, pp. 91–110, 2004.

[4] M. Schroder, H. Rehrauer, K. Seidel, and M. Datcu, "Interactive learning and probabilistic retrieval in remote sensing image archives," *IEEE Trans. Geoscience and Remote Sensing*, vol. 38, no. 5, pp. 2288–2298, 2000.

[5] A. Lorette, X. Descombes, and J. Zerubia, "Texture analysis through a markovian modelling and fuzzy classification: Application to urban area extraction from satellite images," *International Journal of Computer Vision*, vol. 36, no. 3, pp. 221–236, 2000.

[6] A. Winter, H. Maître, N. Cambou, and E. Legrand, "An Original Multi-Sensor Approach to Scale-Based Image Analysis for Aerial and Satellite Images," in *IEEE-ICIP-97*, vol. II, Santa Barbara, CA, USA, 1997, pp. 234–237.

[7] T. Brox and J. Weickert, "A TV flow based local scale measure for texture discrimination," in *ECCV 04*, vol. 2, May 2004, pp. 578–590.

[8] K. Mikolajczyk and C. Schmid, "Scale and affine invariant interest point detectors," *IJCV*, vol. 60, no. 1, pp. 63–86, 2004.

[9] B. Luo, J.-F. Aujol, Y. Gousseau, S. Ladjal, and H. Maître, "Characteristic scale in remote sensing images," in *ICASSP*, vol. II, Toulouse FRANCE, 2006, pp. 809–812.

[10] T. Lindeberg, *Scale-Space Theory in Computer Vision*, ser. Norwell, MA, USA. Kluwer Academic Publishers, 1994.

[11] P. Abry, P. Gonçalvès, and P. Flandrin, *Wavelets, Spectrum Analysis and 1/f Processes*, ser. Lecture Notes in Statistics. Springer, 1995, no. 103, pp. 15–29.

[12] M. Jägerstand, "Saliency maps and attention selection in scale and spatial coordinates: An information theoretic approach," in *Proc. 5th Int. Conf. on Computer Vision*, 1995, pp. 195–202.

[13] J. Sporring, "The entropy of scale-space," in *ICPR*, vol. A, 1996, pp. 900–904.

[14] J. Sporring and J. Weickert, "On generalized entropies and scale-space," in *Scale-Space Theories in Computer Vision*, 1997, pp. 53–64.

[15] T. Kadir and M. Brady, "Scale, saliency and image description," *International Journal of Computer Vision*, vol. 45, no. 2, pp. 83–105, 2001.

[16] C. Woodcock, A. Strahler, and D. Jupp, "The use of variogram in remote sensing II : real digital images," *Remote Sensing and Environment*, vol. 25, pp. 349–379, 1988.

[17] A. Baddeley, *Stochastic Geometry : Likelihood and Computation*. Chapman & Hall / CRC, 1999, ch. Spatial Sampling and Censoring.

[18] M. Lavielle and C. Lévy-Leduc, "Semiparametric estimation of the frequency of unknown periodic functions and its application to laser vibrometry signals," *IEEE Transactions on Signal Processing*, vol. 53, no. 7, pp. 2306–2315, 2005.

[19] J. Koenderink, "The structure of images," *Biological Cybernetics*, vol. 50, pp. 363–370, 1984.

[20] G. Aubert and P. Kornprobst, *Mathematical Problems in Image Processing*, ser. Applied Mathematical Sciences. Springer-Verlag, 2002, vol. 147.

[21] L. Alvarez, F. Guichard, P.-L. Lions, and J.-M. Morel, "Axioms and fundamental equations of image processing," *Arch. for Rational Mechanics*, vol. 123, no. 3, pp. 199–257, 1993.

[22] V. Caselles, B. Coll, and J. M. Morel, "Scale space versus topographic map for natural images," in *Scale-space 97*, Utrecht, 1997.

[23] L. Evans and R. Gariepy, *Measure Theory and Fine Properties of Functions*, ser. Studies in Advanced Mathematics. CRC Press, 1992, vol. 19.

[24] S. Mallat and W. Hwang, "Singularity detection and processing with wavelets," *IEEE Trans. on Information Theory*, vol. 38, no. 2, pp. 617–643, 1992.

[25] B. Luo, J.-F. Aujol, Y. Gousseau, and S. Ladjal, "Interpolation of wavelet features for satellite images with different resolutions," in *IGARSS*, Denver USA, 2006.

[26] Y. Meyer, "Oscillating patterns in image processing and in some nonlinear evolution equations," March 2001, the Fifteenth Dean Jacquelines B. Lewis Memorial Lectures.

Bin Luo Bin Luo has received the Bachelor degree in telecommunication in Wuhan University, Wuhan, China in 2003. He has received the Master degree in applied mathematics and computer vision from École Normale Supérieure de Cachan, Cachan, France in 2004. He is currently Ph.D. student in the Department of Signal and Image Processing, École Nationale Supérieure des Télécommunications (Paris, France). His research interests include remote sensing image formation, data mining, image processing and computer vision.

Jean-François Aujol Jean-François Aujol studied Mathematics at the Ecole Normale Supérieure in Cachan. He received his Ph.D. in Applied Mathematics from Nice-Sophia-Antipolis University in June 2004. In 2004-2005, he was successively an assistant researcher in UCLA (Applied Mathematics Department), and then a research ingeneer at ENST (TSI department) in Paris. Since then, Jean-François Aujol is a scientist researcher with CNRS, at Centre de Mathématiques et de leurs Applications (CMLA, ENS Cachan, CNRS, PRES UniverSud), France. He is interested in mathematical problems related to image processing.

Yann Gousseau Yann Gousseau graduated from École Centrale de Paris in 1995 and obtained the PhD degree in applied mathematics from University Paris Dauphine in 2000. After working as a post-doc at Brown University and École Normale Supérieure de Cachan, he joined École Nationale Supérieure des Télécommunications (Paris, France) as an Associate Professor in 2001. His research interests include the mathematical modeling of natural images, image analysis, computer vision and image processing.

Saïd Ladjal Saïd Ladjal is a former student of the École Normale Supérieure. He received an engineering degree from the ENST and a PhD degree from the ENS Cachan in 2005.

He is currently an associate Professor in the Signal and Image Processing (TSI) Department, ENST. His research intersets include image restoration and blind deconvolution.

Henri Maître Henri MAÎTRE received the engineering degree from the École Centrale de Lyon, France, in 1971, and the Docteur ès Sciences degree in Physics from the University of Paris VI in 1982. He has taught digital picture processing since 1973 at the Ecole Nationale Supérieure des Télécommunications (ENST) in Paris where he is a Professor. His research includes work on image analysis, image understanding and pattern recognition.